Commun. Comput. Phys.
doi: 10.4208/cicp.260715.210316a

Vol. **20**, No. 2, pp. 441-458
August 2016

Investigation of Dielectric Decrement and Correlation Effects on Electric Double-Layer Capacitance by Self-Consistent Field Model

Manman Ma[1,*], Shuangliang Zhao[2] and Zhenli Xu[3]

[1] *Department of Mathematics and Institute of Natural Sciences, Shanghai Jiao Tong University, Shanghai 200240, China.*
[2] *State Key laboratory of Chemical Engineering, East China University of Science and Technology, 200237, Shanghai, China.*
[3] *Institute of Natural Sciences, Department of Mathematics, and MoE Key Lab of Scientific and Engineering Computing, Shanghai Jiao Tong University, Shanghai 200240, China.*

Received 26 July 2015; Accepted (in revised version) 21 March 2016

Abstract. The differential capacitance of electric double-layer capacitors is studied by developing a generalized model of the self-consistent Gaussian field theory. This model includes many-body effects of particles near the interface such as ionic sizes, the order of water alignment and electrostatic correlations, and thus can present more accurate predictions of the electric double-layer structure and hence the capacitance than traditional continuum theories. Analytical simplification of the model and efficient numerical method are introduced, in particular, the approximation of the self-Green's function which describes the self energy of a mobile ion. We show that, when the applied voltage on interfaces is small the dielectric effect of the electrode materials plays an important role. For large voltage, this effect is screened, but the dielectric saturation due to the alignment of the nearby water is shown to be essential. For 2:1 electrolytes, abnormal enhancement on the capacitance due to the dielectric electrode is observed, which is due to the interplay of the image charge effect and Born solvation energy in the self energy of ions.

AMS subject classifications: 65Z05, 65N06, 92E99
Key words: Supercapacitor, many-body effects, Green's function, continuum theory.

1 introduction

For a charged surface in an electrolyte, counterions are attracted to the surface by the electric field. The structure of the screened ions forms the so-called "electric double layer"

*Corresponding author. *Email addresses:* mmm@sjtu.edu.cn (M. Ma), szhao@ecust.edu.cn (S. Zhao), xuzl@sjtu.edu.cn (Z. Xu)

 ©2016 Global-Science Press

https://doi.org/10.4208/cicp.260715.210316a Published online by Cambridge University Press

(EDL) structure. The study of EDLs is of great interest in understanding the electrochemical capacitors (ECs) or supercapacitors because of the rising demand for high power energy storages and the development of blue energy devices [1, 2]. For example, the "capacitive mixing" for harvesting the free energy of solutions has been shown promising for blue energy applications, which are paid great recent theoretical attention such as the effects of different salt concentrations [3], multi-valence [4] and electrode materials [5] to the energy production process. These studies show many-body effects such as short-range size effect and long-range electrostatic correlation play important role in determining the structure of the EDL and the efficiency of energy storages, thus the EDL capacitance can not be accurately described by the classical Poisson-Boltzmann (PB) theory due to the ignorance of these many-body effects.

As a result of the limitations caused by the mean-field treatment, there are many different approaches to extend the PB theory in order to correctly describe the EDL. A simple but widely used extension is the Gouy-Chapman-Stern model [6–8], which considers a charge free layer or the so-called Stern layer near the surface and a diffuse layer beyond that. Another approach is to introduce the ionic steric effects that prevent ions from accumulating near the highly charged surface because of the high ionic densities [9–11] with a local correction of entropic contribution in free energy. Based on this treatment, Kornyshev [12] proposed an analytical formula for EDL capacitance at a metal and ionic liquid interface. Alternately, the density functional theory (DFT) introduces fundamental measure theory [13], which more accurately describes the ion-size effect [14, 15], and thus provides richer phenomena of the EDL capacitance [16].

An important issue for the EDL capacitance is the effect of the inhomogeneity of the dielectric permittivity within the EDL. The dielectric constant of the electrolyte has been shown to depend on both the electric field and ionic concentrations from the experimental results [17, 18]. On one hand, the field dependency of the dielectric function was systematically studied early in the 1950s by Booth [19, 20]. The corresponding Booth model was later introduced into the PB theory [21–23] and the research on the EDL capacitors [24–26]. On the other hand, there will be a decrease of the dielectric constant of solutions when salts are added to them. This is thought as a result of the effective polarizability or solvation of ions when the water molecules around the ions are prevented from orienting against the applied field and hence the dielectric constant of the electrolyte will be reduced. This important property was investigated by Hasted, *et al.* [17], followed by many publications in this field [27–31]. For the related work on the EDL capacitance, the readers are referred to Refs. [32–34]. It is also shown by MD simulations [35–37] that the interfacial dielectric function is closely related to the molecular solvent structure of the surface, and this space-dependent dielectric permittivity can significantly change the ionic distribution surrounding an interface as is observed by primitive-based Monte Carlo calculations [38].

To go beyond the mean field theory such that many-body interactions can be included, a self-consistent field theory by Gaussian variational formulation has been systematically derived [39–41]. The theory presents a better approximation of the potential

https://doi.org/10.4208/cicp.260715.210316a Published online by Cambridge University Press

of mean force by adding the self energy to correct the mean-potential approximation. The self energy is obtained by the solution of the so-called generalized Debye-Hückel (DH) equation, which is a Green's function equation with coefficients nonlinearly depending on the mean ionic densities. The resulted system of partial differential equations is self consistent, and presents a challenging requirement in mathematical analysis and numerical approximations. Different issues, such as the inclusion of ionic size and dielectric effects and the approximate solution, have been frequently discussed in recent publications [42–47]. One important advantage of the theory, comparing with many other liquid state theories including DFT [48,49], is that the dielectric property of the electrode for the EDL capacitors can be directly incorporated into the self energy.

In this work, we investigate the EDL capacitance for an electrode-electrolyte system with variable dielectric permittivity. We consider both the field-dependent dielectric permittivity and the dielectric boundary effect by different electrode materials. Based on the self-consistent theory, we propose a new approach for modeling the EDL capacitance and develop efficient numerical methods to solve the coupled equation system. The outline of the paper is as follows. In Section 2, a self-consistent model is proposed for calculating the EDL capacitance with the inclusion of the effects of ion-ion correlations, image charges and ionic sizes. In Section 3, we develop a hybrid numerical method with an approximated way of evaluating the self energy and solve the coupled equation system with iterative numerical methods. Next, we show in Section 4 the numerical results of EDL capacitance and investigate properties for different surface potentials, bulk densities and dielectric boundaries. Finally, we draw the conclusion in Section 5.

2 Self-consistent field model

We consider a system including a binary electrolyte with 1:1 or 2:1 salts. We assume the hydrated ions are charged spheres of size a_i, each carries a charge at the center of the ion with charge valence z_i ($i=1$ for cations and $i=2$ for anions). The water solvent is treated implicitly but with the relative dielectric function ε depending on the electric field to account for the influence of the ordering of water alignment, the bulk value of which is $\varepsilon_W = 80$. As illustrated in Fig. 1, a planar dielectric surface is located at $x=0$, which separates the space into a dielectric medium of relative permittivity ε_B and the electrolyte occupying the region $x>0$. A constant surface potential V_B is applied on the region $x<0$, which will correspond a uniform surface charge density σ at $x=0$ for the equilibrium system. The dielectric surface is thought as an electrode in an EDL capacitor system. The differential capacitance of the electrode-electrolyte system is defined by,

$$C_{\text{diff}} = \frac{d\sigma}{dV_B}, \tag{2.1}$$

where σ is determined by the charge neutrality condition via the electric potential Φ, given by,

$$\sigma = -\varepsilon_0 \varepsilon \left.\frac{d\Phi}{dx}\right|_{x=0}. \tag{2.2}$$

https://doi.org/10.4208/cicp.260715.210316a Published online by Cambridge University Press

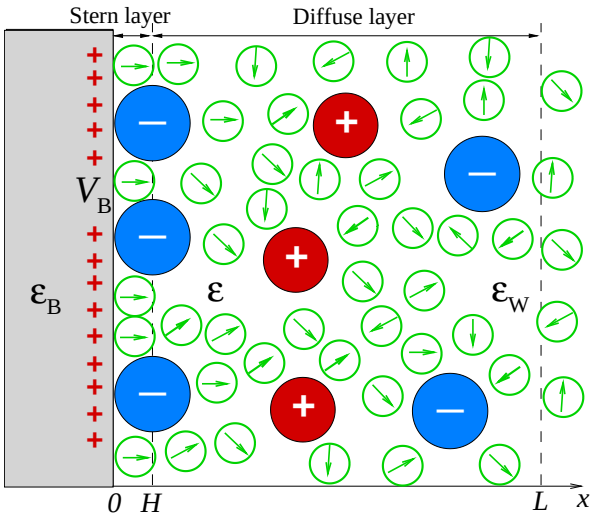


Figure 1: Schematic representation of the electrolyte near a dielectric surface with an applied voltage: The red and blue balls denote the hydrated cations and anions, respectively. Water molecules are represented as green circles with arrows showing the direction of dipoles, which are described by electric-field-dependent dielectric permittivity in the continuum theory.

Here $\varepsilon_0\varepsilon$ is the local dielectric permittivity of electrolyte, and ε_0 is the vacuum permittivity. The capacitance can then be measured by calculating the surface charge density with increase of the surface voltage.

In order to describe the electric potential distribution by the continuum theory, we divide the electrolyte into two parts at $x=H$ due to the finite ion size of the counterions: The Stern layer for $0<x<H$, and the diffuse layer for $x>H$. The Stern layer could also be thought as a charge free layer and the diffuse layer consists of mobile ions. The property of Stern layer is of importance for the EDL capacitor, and the inclusion of it is crucial for theoretical understanding of the capacitance [25, 50, 51]. For the diffusion layer, the self-energy modified Poisson-Boltzmann (PB) equation for the electric potential Φ coupled with a Green's function [39–41, 46] is used. The governing equations are as following,

$$\begin{cases} -\varepsilon_0\nabla\cdot\varepsilon\nabla\Phi=0, & 0<x<H, \\ -\varepsilon_0\nabla\cdot\varepsilon\nabla\Phi=\sum\limits_{i=1,2} z_i e\widetilde{c}_{i0}e^{-\beta U_i}, & H<x<L, \\ U_i=z_i e\Phi+\dfrac{1}{2}z_i^2e^2u_i, \end{cases} \tag{2.3}$$

subject to some boundary conditions to be discussed later on, where e is the elementary charge, $\beta=1/k_BT$ is the inverse thermal energy. Here, $\widetilde{c}_{i0}=c_{i0}e^{\frac{1}{2}\beta z_i^2e^2u_i(\infty)}$, z_i and c_{i0} are the valency and the bulk number density of the ith ion, and L is a length much larger than the Debye length. The self energy $\frac{1}{2}z_i^2e^2u_i$ in the diffusion layer accounts for the fluctuation contribution in the free energy cost when moving a test ion from the vacuum region into

https://doi.org/10.4208/cicp.260715.210316a Published online by Cambridge University Press

its current position. It is defined by the self Green's function,

$$u_i = \lim_{\mathbf{r}' \to \mathbf{r}} \left[G_i(\mathbf{r},\mathbf{r}') - G_0(\mathbf{r},\mathbf{r}') \right], \tag{2.4}$$

where G_0 is the free-space Green's function described by $-\varepsilon_0 \nabla^2 G_0(\mathbf{r},\mathbf{r}') = \delta(\mathbf{r},\mathbf{r}')$. The Green's function G_i is described by a generalized Debye-Hückel (DH) equation [43],

$$-\varepsilon_0 \nabla \cdot \varepsilon_i(\mathbf{r},\mathbf{r}') \nabla G_i(\mathbf{r},\mathbf{r}') + 2 I_i(\mathbf{r},\mathbf{r}') G_i(\mathbf{r},\mathbf{r}') = \delta(\mathbf{r},\mathbf{r}'), \tag{2.5}$$

where the dielectric function ε_i and the local ionic strength I_i are expressed as,

$$\varepsilon_i(\mathbf{r},\mathbf{r}') = \begin{cases} 1, & |\mathbf{r}-\mathbf{r}'| < a_i, \\ \varepsilon(\mathbf{r}), & \text{otherwise}, \end{cases} \tag{2.6}$$

$$I_i(\mathbf{r},\mathbf{r}') = \begin{cases} 0, & |\mathbf{r}-\mathbf{r}'| < a_i \ \text{ or } \ x < H, \\ I(\mathbf{r}), & \text{otherwise}, \end{cases} \tag{2.7}$$

and the ionic strength

$$I(\mathbf{r}) = \frac{1}{2} \beta e^2 \sum_i z_i^2 c_i. \tag{2.8}$$

The local density of ions is given by,

$$c_i(\mathbf{r}) = \widetilde{c}_{i0} e^{-\beta \left[z_i e \Phi(\mathbf{r}) + \frac{1}{2} z_i^2 e^2 u_i(\mathbf{r}) \right]}, \tag{2.9}$$

as shown in the PB equation. It can be noted that the ionic size effect has been involved in above equations. The Green's function equation has to be solved within the whole domain in order to include the effects of the dielectric boundary, although we only need solutions in the electrolyte.

The relative dielectric function is a constant within the electrode boundary, $\varepsilon(\mathbf{r}) = \varepsilon_{\mathrm{B}}$ for $x < 0$. In the electrolyte, the solvent dipoles are highly oriented under large electric fields and the dielectric saturation is caused. The Booth model for the field-dependent dielectric permittivity is considered [19,20,23],

$$\varepsilon(\mathbf{r}) = \varepsilon(E) = 1 + \frac{p_0 c_d \mathscr{L}(\beta p_0 E)}{\varepsilon_0 E}, \tag{2.10}$$

with the field strength $E = |\nabla \Phi|$, the Langevin function $\mathscr{L}(x) = \coth x - 1/x$, and p_0 and c_d being the permanent dipole moment of a solvent molecule and its number density. In the case of water solvent, we have the limit in bulk electrolytes $\varepsilon(E \to 0) = 1 + \beta p_0^2 c_d / 3\varepsilon_0 = \varepsilon_{\mathrm{W}}$, giving that $\beta p_0^2 c_d = 3\varepsilon_0(\varepsilon_{\mathrm{W}} - 1)$. In the derivation, the fluctuation of the dipolar density is neglected (see Ref. [52] for possible consequence), which should not exclude the important physics that we are interested in.

https://doi.org/10.4208/cicp.260715.210316a Published online by Cambridge University Press

At $x=0$, the electric potential is given as a constant $\Phi|_{x=0}=V_B$, and this equivalently gives a boundary condition at the Stern layer by using the continuities of the electric potential and displacement, in a Robin type:

$$\left(-H\frac{\partial\Phi}{\partial x}+\Phi\right)\Big|_{x=H}=V_B. \tag{2.11}$$

Again, since the Stern layer is charge free, the surface charge density σ can be determined at $x=H$ with the same expression as Eq. (2.2), after solving the modified PB equation in the interval $x\in[H,L]$ subject to the decaying boundary condition at $x=L$.

3 Numerical methods

The most challenging component in the solution of the self-consistent field model is to solve the self energy u_i from the Green's function equation (2.4) and (2.5). In principle, the discretization scheme of this high dimensional problem can be solved by the selected inversion algorithm [53, 54]. The multiscale character of the problem leads to a need of small grid size in the numerical scheme, much smaller than the ionic radius, limiting the capability of the algorithm. The Green's function has to be well treated, e.g., by asymptotic methods [41, 46], before the discretization. Following [46], we approximate the self energy asymptotically as the sum of two contributions,

$$u_i\approx\frac{\widetilde{u}}{1-4\pi\varepsilon_0\varepsilon a_i\widetilde{u}}+\frac{1}{4\pi\varepsilon_0 a_i}\left(\frac{1}{\varepsilon}-1\right), \tag{3.1}$$

where

$$\widetilde{u}=\lim_{\mathbf{r}'\to\mathbf{r}}(\widetilde{G}-\widetilde{G}'), \tag{3.2}$$

$\widetilde{G}$ and $\widetilde{G}'$ are Green's functions defined by,

$$-\varepsilon_0\nabla\cdot\varepsilon(\mathbf{r})\nabla\widetilde{G}+2I(\mathbf{r})\widetilde{G}=\delta(\mathbf{r}-\mathbf{r}'), \tag{3.3}$$

$$-\varepsilon_0\varepsilon(\mathbf{r}')\nabla^2\widetilde{G}'=\delta(\mathbf{r}-\mathbf{r}'). \tag{3.4}$$

We shall see that solving Eq. (3.3) becomes easier since the smaller scale $\mathcal{O}(a)$ is removed. $\widetilde{u}$ is utilized to approximate the global correlation energy which is the first term in Eq. (3.1) with ionic size effect, and the second term is the generalized Born solvation energy to describe the free energy variation in a medium of variable permittivity. From approximate point of view, we make a constraint on the correlation energy and avoid the numerical instability which may occur in the limit of $a_i\to 0$.

The solution of Eq. (3.4) can be found exactly, but we solve it numerically in order to cancel the numerical singularity and ensure the consistent numerical accuracy with Eq. (3.3). A fast and efficient finite difference method for solving $\widetilde{G}$ and $\widetilde{G}'$ has been developed in our previous work [43]. We reduce the dimensions by applying the polar

https://doi.org/10.4208/cicp.260715.210316a Published online by Cambridge University Press

symmetric Fourier transform to the Green's function equation. Recall that $\varepsilon(x)=\varepsilon_B$ for $x<0$ and $I(x)=0$ for $x<H$. After the Fourier transform with respect to $y-y'$ and $z-z'$, we have the corresponding frequency Green's functions $\widehat{G}$ and $\widehat{G}'$ with the frequency ω,

$$\left[-\varepsilon_0\partial_x\varepsilon(x)\partial_x+\varepsilon_0\varepsilon(x)\omega^2+2I(x)\right]\widehat{G}(\omega;x,x')=\delta(x-x')/2\pi, \tag{3.5}$$

$$\left[-\varepsilon_0\varepsilon(x')\partial_{xx}+\varepsilon_0\varepsilon(x')\omega^2\right]\widehat{G}'(\omega;x,x')=\delta(x-x')/2\pi. \tag{3.6}$$

Finite difference method is utilized to discretize Eqs. (3.5) and (3.6) with central differences for the derivatives of $\widehat{G}$ and $\widehat{G}'$, and Kronecker δ_{ij} for $\delta(x_i-x_j)$ since the function is defined on lattices. These equations are solved within the domain $-L<x<2L$ such that the dielectric boundary effect has been accurately taken into account. We then compute $\widetilde{u}$ by the inverse Fourier transform

$$\widetilde{u}(x_j)=\int_0^\infty\left[\widehat{G}_{jj}(\omega)-\widehat{G}'_{jj}(\omega)\right]\omega d\omega, \tag{3.7}$$

where the $\widehat{G}_{jj}(\omega)$ and $\widehat{G}'_{jj}(\omega)$ are the diagonal elements of the frequency Green's functions, which are usually solved by sparse inversion techniques [53, 54]. The numerical integration of Eq. (3.7) should give us $\widetilde{u}$ and hence the total self energy u_i after adding the local Born energy.

Since the self energy can be approximated in an efficient way, a self-consistent iteration algorithm is applied for the integration of the modified PB equation with the state equations by numerical approach proposed in Ref. [44], as,

$$u_i^{(k)}=\frac{\widetilde{u}^{(k)}}{1-4\pi\varepsilon_0\varepsilon^{(k)}a_i\widetilde{u}^{(k)}}+\frac{1}{4\pi\varepsilon_0 a_i}\left(\frac{1}{\varepsilon^{(k)}}-1\right), \tag{3.8}$$

$$-\varepsilon_0\nabla\cdot\varepsilon^{(k+1)}\nabla\Phi^{(k+1)}=\sum_{i=1,2}z_ie\widetilde{c}_{i0}e^{-\beta U_i^{(k+1)}}, \tag{3.9}$$

$$U_i^{(k+1)}=z_ie\Phi^{(k+1)}+\frac{1}{2}z_i^2e^2u_i^{(k)}, \tag{3.10}$$

for k=0,1,2,$\cdots$,K, where the superscript (k) represents the index of iteration step. Namely, the algorithm is composed by the following steps: (1) Calculate $u_i^{(k)}$ in the kth loop with given $c_i^{(k)}$ and $\varepsilon^{(k)}$; (2) Given $u_i^{(k)}$, solve the modified PB equation to obtain $\Phi^{(k+1)}$; (3) Calculate $c_i^{(k+1)}$ and $\varepsilon^{(k+1)}$ by using $\Phi^{(k+1)}$, then return to (1). The iterative steps are performed until the convergence criteria $|u_i^{(k+1)}-u_i^{(k)}|<\delta$ is arrived, where δ is a small tolerant value.

In step (2),the modified PB equation (3.9) should be solved in an efficient way. Since it is nonlinear, we solve it by an iterative scheme. Let

$$\gamma(\mathbf{r})=\frac{|\sum_{i=1,2}z_iec_i|}{|\Phi|+\delta/(\beta e)} \tag{3.11}$$

https://doi.org/10.4208/cicp.260715.210316a Published online by Cambridge University Press

be a relaxation function. During the kth loop of the self-consistent iteration, the scheme for the $[l]$th step of the sub-iteration is

$$-\varepsilon_0\nabla\cdot\varepsilon^{[l]}\nabla\Phi^{[l+1]}-\gamma^{[l]}\Phi^{[l+1]}=\sum_{i=1,2}z_ie\widetilde{c}_{i0}e^{-\beta\left(z_ie\Phi^{[l]}+\frac{1}{2}z_i^2e^2u_i^{(k)}\right)}-\gamma^{[l]}\Phi^{[l]}, \tag{3.12}$$

which is to find $\Phi^{[l+1]}$ by solving a linear system. This iteration stops when the convergence criteria $|\Phi^{[l+1]}-\Phi^{[l]}|<\delta$ is arrived. We take $\delta=10^{-8}$ for the convergence criteria and the small value in the relaxation function.

4 Results and discussion

Based on the numerical results of the SCF model, we study the capacitance of EDLs in 1:1 and 2:1 binary electrolytes, i.e., $z_1:z_2=1:-1$ and $2:-1$. We mainly consider cases of electrolytes with three different bulk densities of salts: $c_{\rm B}=1$ M, 100 mM and 10 mM, thus the ionic bulk densities are $c_{10}=|z_2|c_B=c_B$ and $c_{20}=|z_1|c_B$. The relative dielectric constant of bulk water is $\varepsilon_{\rm W}=80$ and the Bjerrum length is $\ell_{\rm B}=0.714$ nm at room temperature. The dielectric ratio $\varepsilon_{\rm B}/\varepsilon_{\rm W}=1$ is first studied in Sections 4.1 and 4.2 and the dielectric boundary effect is involved at last by performing calculations for different ratios of $\varepsilon_{\rm B}/\varepsilon_{\rm W}$. The dimensionless surface potential $V=\beta eV_{\rm B}$ is used hereafter, while all other properties in the results are dimensional.

4.1 Significant effect of electrostatic correlation at low voltages

In the first group of calculations, we use symmetric 1:1 electrolytes with uniform ionic sizes $a_1=a_2=0.4$ nm. The mean-field (MF) model is also calculated, which ignores the self-energy effect; namely it is just the same model as the SCF model but setting the self energy $u_i=0$. The comparison between the SCF and the MF models is performed to investigate the role of self energy. The effects of the field-dependent dielectric permittivity are included in both models. Since the MF model ignores the ionic size and other specific effects, by the comparison between both models, the influence of the self energy on the capacitance and ionic distribution can be observed and analyzed.

The differential capacitance $C_{\rm diff}$ *versus* V curves for three salt densities are present in Fig. 2(a), where both the MF and SCF results are plotted. Both theories predict symmetric curves about $V=0$ since both the ionic valency and size are symmetric. For the MF model, the change from the bell shape to the camel shapes is observed as the bulk concentration decreases, while the SCF results present more obvious camel shapes for all three curves. The non-monotonic variation of the differential capacitance with the surface potential is ascribed to the saturation of surface charge at higher surface potential, which makes the bending of the curves. This owes to the dielectric decrement with the increase of the surface potential from the Booth model. Ignoring this effect of the dielectric decrement, the MF model predicts monotonically increasing capacitance curves with the surface potential (not shown).

https://doi.org/10.4208/cicp.260715.210316a Published online by Cambridge University Press

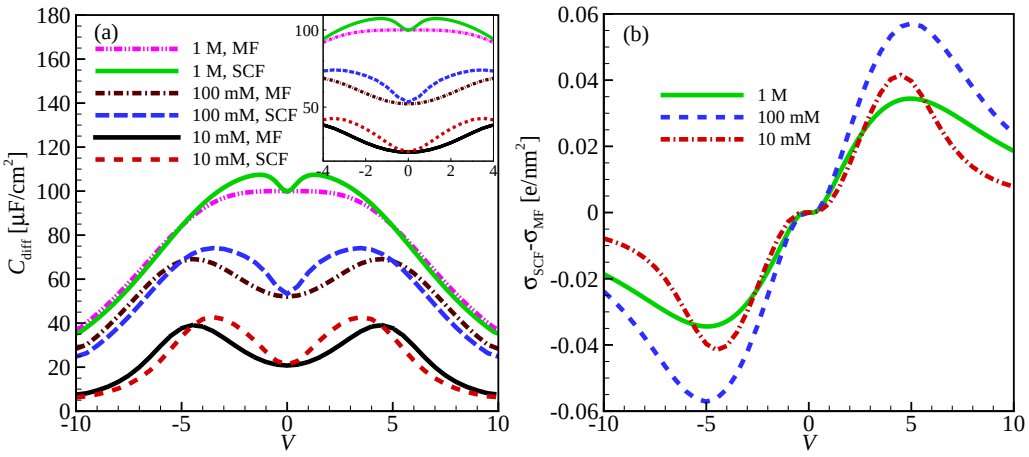


Figure 2: Monovalent electrolytes of uniform size $a_1 = a_2 = 0.4$ nm by the MF and SCF theory. (a) Capacitance versus surface potential curves; and (b) the difference of the surface charge densities between two models.

The self energy affects the capacitance in different ways for weak and strong surface potentials. Fig. 2(a) shows that the self energy in the SCF model enhances the differential capacitance at small potentials while reduces it after a critical potential $V_c \sim \pm 4.5$ ($k_B T/e$). Additional data by comparing the surface charge density as the function of the voltage shows the self energy in the SCF model always enhances the surface charge density for a 1:1 symmetric electrolyte, as shown in Fig. 2(b). The maximum enhancement (or the peaks) appears in the critical potential which is slightly different for variable salt concentrations. This enhancement can be understood as the competition between electrostatic correlation and the solvation energy. The correlation effect enhances the charge aggregation in the double layer, leading to a higher surface charge than the MF model. When the surface voltage is increased, the dielectric decrement results in higher solvation expense by moving an ion to the double layer, which then diminishes the aggregation effect. It should be remarked that the results of small voltages (embedded subplot in Fig. 2(a)) are physically more interesting since the high-voltage condition is difficult to achieve in electrochemical experiments due to the electrolysis of water.

4.2 High-valence and small ions enlarge correlation effects

We now consider the electrolytes with asymmetric valences or ionic sizes. Fig. 3 shows the voltage-capacitance curves for four groups of electrolytes: One group of 1:1 salts with asymmetric sizes (a), and three groups of 2:1 salts with symmetric and asymmetric sizes (b-d).

The ionic size effect is of great recent interest due to its influence on ionic solvation and short-range correlation. Even for symmetric valences, voltage-capacitance curves may not be symmetric in real experiments since cations and coions usually have different sizes, as is shown in Fig. 3(a), where the radii of cations and anions are 0.3 and 0.4

https://doi.org/10.4208/cicp.260715.210316a Published online by Cambridge University Press

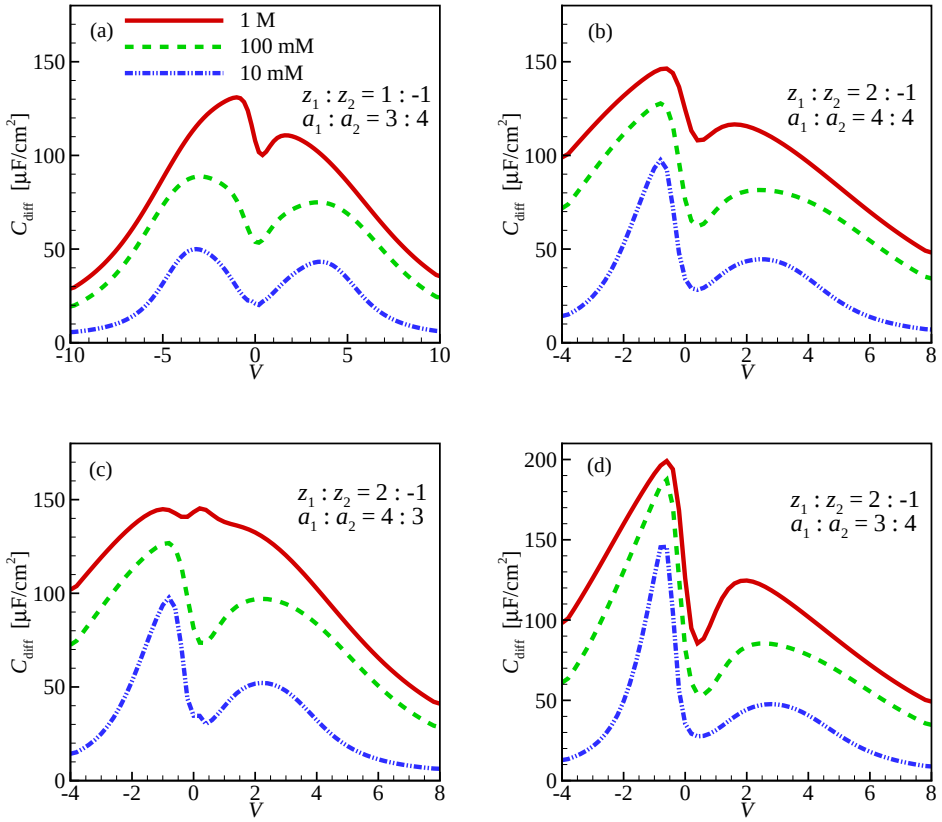


Figure 3: EDL capacitance from the SCF model for electrolytes of asymmetric valence or nonuniform ion size. (a) 1:1 electrolyte, $a_1=0.3$ nm and $a_2=0.4$ nm; (b) 2:1 electrolyte, $a_1=a_2=0.4$ nm; (c) 2:1 electrolyte, $a_1=0.4$ nm and $a_2=0.3$ nm; (d) 2:1 electrolyte, $a_1=0.3$ nm and $a_2=0.4$ nm.

nm, respectively. Worth noting is that smaller cations make the left wings corresponding to negative electrodes steeper and the left local maximums of differential capacitance with negative potentials bigger. We shall also observe that, for the lower bulk salt concentration, the larger range of V over which the curve is symmetric. This feature was pointed out by Macdonald in [25] from summarizing the experimental data [55]. It is remarked that the MF model always predicts symmetric curves and thus can be usable only for weak surface voltages. The breaking of symmetry on the valence should also significantly change the shape of the curves, as is shown in Fig. 3(b) for 2:1 salts of uniform size. The obvious asymmetric shape about $V=0$ can be observed. The maximums of differential capacitance are at negative potentials, ascribed to the strong ion correlation between divalent cations near negative electrodes.

The 2:1 salts with asymmetric ionic sizes show more complex behaviors. Fig. 3(c) illustrates that the smaller anions cause the steeper curves of C_{diff} at positive potentials,

https://doi.org/10.4208/cicp.260715.210316a Published online by Cambridge University Press

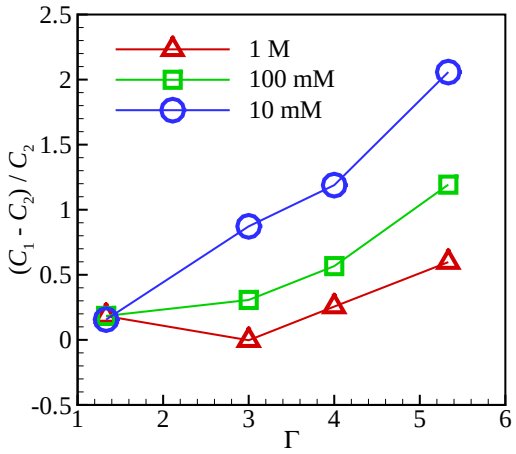


Figure 4: The relative difference of the capacitance peaks as a function of the ratio $\Gamma = s_1/s_2$ with $s_i = z_i^2/a_i$ being a measure of ion asymmetry. C_1 and C_2 are the left and right peaks of the differential capacitance for the simulated cases.

compared to the results of uniform size in Fig. 3(b). As a result, the right local maximum of C_{diff} for positive electrode is enhanced and the difference of the two peaks is reduced. This can be ascribed to the cancellation of effects by asymmetric valencies and ionic sizes. Since both cases have the same cation radius, no obvious difference is observed for the curves at negative electrodes comparing the left peaks. In the last case presented in Fig. 3(d), wherein $a_1 = 0.3$ nm and $a_2 = 0.4$ nm are taken such that the divalent cations are smaller, it can be observed the steeper curves and larger local maximums appear at negative electrodes because of the significant enhancement by the smaller cations.

To summarize, increasing ion correlations could enhance the EDL capacitance, and larger valence and smaller ionic size could increase the correlation part of the self energy (the first term of Eq. (3.1)). At the large voltage, this effect can be significantly reduced by the dielectric decrement (the second term of Eq. (3.1)) due to the strong electric field in the EDL. Since the reverse of the capacitance is the result of the increase of the Born solvation energy, we define an inverse length $s_i = z_i^2/a_i$ for the ith species and use the ratio $\Gamma = s_1/s_2$ to denote the asymmetry of electrolytes, in order to analyze the interplay between two effects. Fig. 4 presents the relative differences of two peaks (C_1 and C_2) for all the simulated systems *versus* the value of parameter Γ for the three bulk concentrations. These relative differences can reflect the degree of asymmetry in the distribution of differential capacitance depicted in Fig. 3 and are shown to be well related to the defined ratio Γ, e.g., the differences monotonically increase with Γ for the curves of low and mediate salt condensations. The curve for 1 M electrolytes does not obey the monotonicity at small Γ regime, mostly because the ion correlation is strong and the Born energy makes less important contribution in the self energy expression Eq. (3.1) in the dense system at low surface voltages.

https://doi.org/10.4208/cicp.260715.210316a Published online by Cambridge University Press

4.3 Abnormal enhancement of capacitance due to low-dielectric electrode

In previous sections, we have fixed the dielectric constant of the electrode as the value of the bulk water $\varepsilon_B = \varepsilon_W$ to neglect the effect of dielectric boundary. This effect may be significantly important in many EDL systems with low surface voltages. Since it ignores this effect, it may provide inaccurate prediction of the EDL structure with the presence of the dielectric mismatch between the electrode and the electrolyte. Unlike in the DFT studies [48,49], the dielectric-boundary effect has been included in the self energy of the SCF model, which can be roughly approximated by the WKB approximation [42,43] using image charges. In the WKB approximation, the dielectric self energy can be decomposed into two contributions. One is the depletion energy about $\propto -\widetilde{\kappa}(x)$ where $\widetilde{\kappa}(x)$ is the effective inverse screening length with detailed definition in [43]. Closer to an interface of weak voltage, weaker is the screening effect thus smaller is $\widetilde{\kappa}(x)$. The other one is due to the image charge effect, which is proportional to the dielectric jump between the electrode and the electrolyte $\gamma = (\varepsilon_W - \varepsilon_B)/(\varepsilon_W + \varepsilon_B)$, and is thus repulsive when $\varepsilon_B < \varepsilon_W$ and attractive when $\varepsilon_B > \varepsilon_W$. For the former case, both contributions are repulsive, leading to a strong depletion zone near the interface, e.g., the air/electrolyte interface [56] and models with ionic specific effects [57–59]. The later case may be complicated, but is very important in the capacitor community since most of electrodes are made of high dielectric materials such as metals.

In Fig. 5, we calculate the ion densities for 1:1 and 2:1 salts near a neutral electrode of dielectric constant $\varepsilon_B = 20\varepsilon_W$. The image charge contribution is attractive to ions, in contrast to the repulsive contribution from the depletion energy, leading to different double layer structures with the increase of salt densities. For low salt condensation, the image charge attraction dominates and thus the charge density near the interface is higher than the bulk value. With the increase of the condensation, the image charge effect becomes

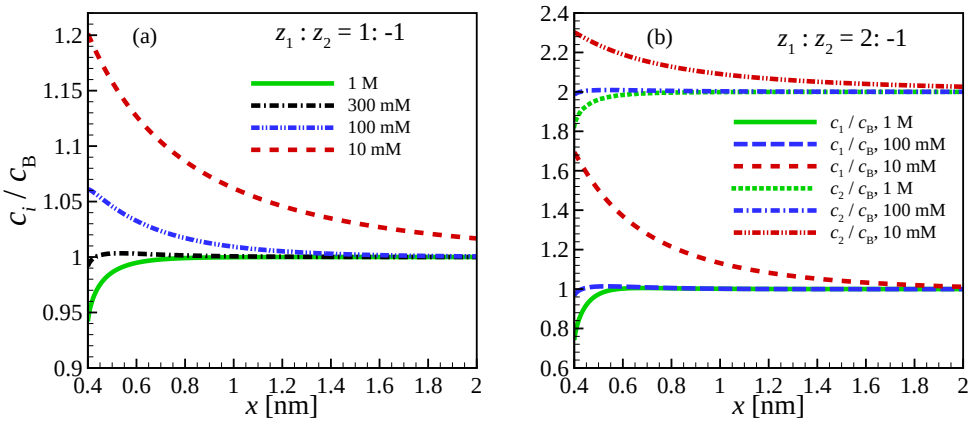


Figure 5: Relative ion densities near neutral surfaces for (a) 1:1 and (b) 2:1 electrolytes of uniform size $a_1 = a_2 = 0.4$ nm. The dielectric ratio $\varepsilon_B/\varepsilon_W = 20$.

https://doi.org/10.4208/cicp.260715.210316a Published online by Cambridge University Press

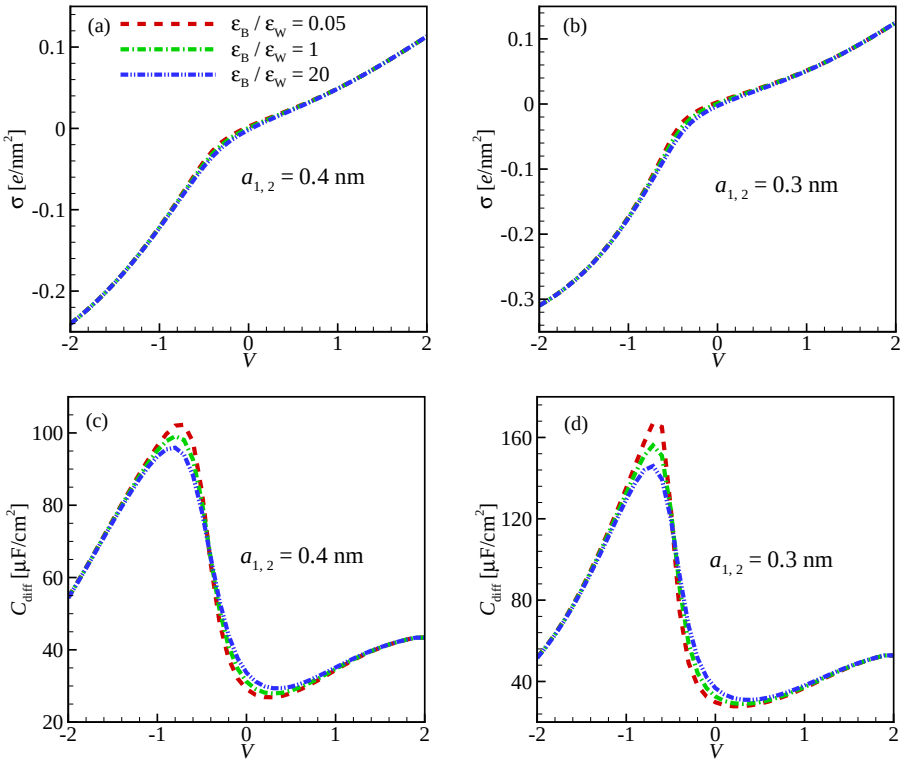


Figure 6: Surface charge density and differential capacitance *versus* surface potential curves with varying the dielectric constant of the electrode for $c_B = 10$ mM. (a, c) $a_1 = a_2 = 0.4$ nm; and (b, d) $a_1 = a_2 = 0.3$ nm.

weaker, and thus the EDL tends to form a depletion zone. For an appropriate bulk concentration, $c_B = 300$ mM for 1:1 electrolytes and 100 mM for 2:1 electrolytes, both image charge and depletion contributions are complementary and the slightly non-monotonic curves are observed.

The image charge effect could be a mechanism to alternate the strength of the differential capacitance. Considering the dependence of the self energy on the valency is quadratic, we study 2:1 electrolytes of $c_B = 10$ mM, since the low bulk concentration reduces the screening of image charge effect. We have assumed the thickness of the Stern layer (H) to be the radius of hydrated ions, however, the constant thickness of the charge free layer is not exactly what was observed experimentally. When ions are attracted to the dielectric boundary, they may get partially or fully dehydrated and be forced to get closer to the surface. Beyond the Stern model, more theories for the thickness of the charge free layer were discussed such as the triple-layer model by Grahame [60], and dielectric-dependent model by MacDonold [25]. For the image charge effect on the complex structure of the charge free layer, it may be significant to investigate the influence of the thickness of the charge free layer. For this, we set $H = a$ and take two sets of radii

https://doi.org/10.4208/cicp.260715.210316a Published online by Cambridge University Press

$a=0.4$ and 0.3 nm, and the size of cations and anions are uniform since the size asymmetry should be a less important factor for dilute electrolyte. The capacitance and surface charge density as functions of V are presented in Fig. 6 for different $\varepsilon_B/\varepsilon_W$. We calculate the results up to $|V|=2$ as we can observe the consistency of curves with different ratios when $|V|$ becomes large.

For negative electrode voltages, cations are attracted to the surface due to the electrostatic interaction between the ions and the surface. However, in the case of low electrode permittivity ($\varepsilon_B/\varepsilon_W=0.05$), the image charges are repulsive to ions near the interface. Cations (counterions) are of higher valency than the anions (coions) and thus are pushed further away from the electrode surface by the image charges of itself. This leads to a cancellation of the attraction energy of cations and a compensation by the coions near the surface. The net charge density will be smaller for low surface voltage, in comparison with the case of mediate and high electrode permittivity. For positive voltages, on the contrary, higher-valent coions are pushed further away from the surface by the image charges. This leads to a compensation of counterions near the surface, increasing the net charge density. In this case, the charge inversion phenomenon could take place even for weakly charged surface [47]. From the curves of surface charge density, we could observe that the positive surface charge density is larger than that of $\varepsilon_B/\varepsilon_W=1$ for positive potentials. The surface charge density profiles for $\varepsilon_B/\varepsilon_W=0.05$ are always over the profiles for $\varepsilon_B/\varepsilon_W=1$, while the differential capacitance is enhanced near the left peak and reduced near the middle valley. When the electrode permittivity is high, $\varepsilon_B/\varepsilon_W=20$, the image charge force is attractive to ions. As a result, the image charge effect indicates opposite trends for differential capacitances in comparison to the case of $\varepsilon_B/\varepsilon_W=0.05$.

By comparing the results of $H=0.4$ nm with those of $H=0.3$ nm, qualitatively similar phenomena are observed, but the effect of image charges is significantly enhanced, e.g., the maximal relative difference of differential capacitance between $\varepsilon_B/\varepsilon_W=0.05$ and $\varepsilon_B/\varepsilon_W=20$ is near 16%, larger than 6% for the case of $H=0.4$ nm. This stronger effect should be ascribed to that the smaller distance between counterions in the EDL and the surface.

In Fig. 7, we show the maximal differential capacitance $C_{\max}$ curves *versus* the ratio $\varepsilon_B/\varepsilon_W$. The significant variations due to the dielectric ratios can be observed for dilute electrolytes $c_B=10$ and 100 mM. The maximal capacitance decreases with the increase of the dielectric ratio. This is counterintuitive since the capacitance is often higher with the increase of the electrode permittivity. For dense electrolytes $c_B=1$ M, we can not obtain distinct differences for different dielectric ratios because of the strong screening effects of image charges by mobile ions.

5 Conclusions

In this work, we have presented numerical investigations on the EDL capacitance based on a self-consistent field model which includes the effects of ionic sizes, varying per-

https://doi.org/10.4208/cicp.260715.210316a Published online by Cambridge University Press

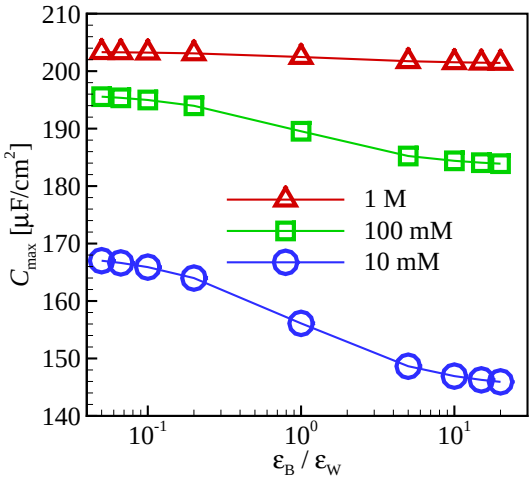


Figure 7: The maximal capacitance *versus* the ratio of dielectric constants for different bulk concentrations, $a_1 = a_2 = 0.3$ nm.

mittivity and electrostatic correlations between ions. We have illustrated the significant influence of these effects on the EDL capacitance by numerical calculations for different ionic concentrations, sizes, valences and dielectric boundaries.

We have compared our model with the classical PB theory to show the obvious improvements of the self-consistent field model. The results show the mean-field theory underestimates the capacitance near the zero voltage due to the ignorance of the ion correlation. We also demonstrate that the EDL capacitance sensitively depends on the valence and the ionic size, and thus it is necessary to use a model with correct treatment of these effects in order to make accurate predictions of the capacitance.

Acknowledgments

M.M. and Z.X. acknowledge the financial support from the Natural Science Foundation of China (Grant Nos. 11571236 and 91130012), Youth Talents Program by Chinese Organization Department, and the HPC center of Shanghai Jiao Tong University. S.Z. acknowledges the support provided by the Shanghai Science and Technology Committee Rising-Star Program (Grant No. 14QA1401300).

References

[1] J. Huang, B. G. Sumpter, V. Meunier, Theoretical model for nanoporous carbon supercapacitors, Angew. Chem. Int. Ed. 47 (3) (2008) 520–524.
[2] M. V. Fedorov, A. A. Kornyshev, Ionic liquids at electrified interfaces, Chem. Rev. 114 (2014) 2978–3036.

https://doi.org/10.4208/cicp.260715.210316a Published online by Cambridge University Press

[3] R. A. Rica, R. Ziano, D. Salerno, F. Mantegazza, R. van Roij, D. Brogioli, Capacitive mixing for harvesting the free energy of solutions at different concentrations, Entropy 15 (4) (2013) 1388–1407.
[4] M. M. Fernández, S. Ahualli, G. R. Iglesias, F. González-Caballero, Á. V. Delgado, M. Jiménez, Multi-ionic effects on energy production based on double layer expansion by salinity exchange, J. Colloid Interf. Sci. 446 (2015) 307–316.
[5] G. R. Iglesias, M. M. Fernández, S. Ahualli, M. L. Jiménez, O. P. Kozynchenko, Á. V. Delgado, Materials selection for optimum energy production by double layer expansion methods, J. Power Sources 261 (2014) 371–377.
[6] G. Gouy, Constitution of the electric charge at the surface of an electrolyte, J. Phys. 9 (1910) 457–468.
[7] D. L. Chapman, A contribution to the theory of electrocapillarity, Phil. Mag. 25 (1913) 475–481.
[8] O. Stern, The theory of the electrolytic double-layer, Zeit. Elektrochem 30 (1924) 508–516.
[9] I. Borukhov, D. Andelman, H. Orland, Steric effects in electrolytes: A modified Poisson-Boltzmann equation, Phys. Rev. Lett. 79 (1997) 435–438.
[10] D. Ben-Yaakov, D. Andelman, D. Harries, R. Podgornik, Beyond standard Poisson–Boltzmann theory: Ion-specific interactions in aqueous solutions, J. Phys.: Condens. Matter 21 (2009) 424106.
[11] B. Li, Continuum electrostatics for ionic solutions with nonuniform ionic sizes, Nonlinearity 22 (2009) 811–833.
[12] A. A. Kornyshev, Double-layer in ionic liquids: paradigm change?, J. Phys. Chem. B 111 (2007) 5545–5557.
[13] Y. Rosenfeld, Free-energy model for the inhomogeneous hard-sphere fluid mixture and density-functional theory of freezing, Phys. Rev. Lett. 63 (9) (1989) 980–983.
[14] J. Wu, Density functional theory for liquid structure and thermodynamics, in: Molecular Thermodynamics of Complex Systems, Vol. 131 of Structure and Bonding, Springer Berlin Heidelberg, 2009, pp. 1–73.
[15] S. Zhao, Y. Liu, X. Chen, Y. Lu, H. Liu, Y. Hu, Unified framework of multiscale density functional theories and its recent applications, in: Mesoscale Modeling in Chemical Engineering Part II, Vol. 47 of Advances in Chemical Engineering, Academic Press, 2015, pp. 1 – 83.
[16] D.-e. Jiang, Z. Jin, J. Wu, Oscillation of capacitance inside nanopores, Nano letters 11 (12) (2011) 5373–5377.
[17] J. Hasted, D. Ritson, C. Collie, Dielectric properties of aqueous ionic solutions. Parts I and II, J. Chem. Phys. 16 (1) (1948) 1–21.
[18] A. Lyashchenko, A. Y. Zasetsky, Complex dielectric permittivity and relaxation parameters of concentrated aqueous electrolyte solutions in millimeter and centimeter wavelength ranges, J. Molecular Liquids 77 (1) (1998) 61–75.
[19] F. Booth, The dielectric constant of water and the saturation effect, J. Chem. Phys. 19 (4) (1951) 391–394.
[20] F. Booth, Dielectric constant of polar liquids at high field strengths, J. Chem. Phys. 23 (3) (1955) 453–457.
[21] V. Paunov, R. Dimova, P. Kralchevsky, G. Broze, A. Mehreteab, The hydration repulsion between charged surfaces as an interplay of volume exclusion and dielectric saturation effects, J. Colloid Interf. Sci. 182 (1) (1996) 239–248.
[22] A. Abrashkin, D. Andelman, H. Orland, Dipolar Poisson-Boltzmann equation: ions and dipoles close to charge interfaces, Phys. Rev. Lett. 99 (7) (2007) 077801.

https://doi.org/10.4208/cicp.260715.210316a Published online by Cambridge University Press

[23] D. Frydel, M. Oettel, Charged particles at fluid interfaces as a probe into structural details of a double layer, Phys. Chem. Chem. Phys. 13 (9) (2011) 4109–4118.
[24] Y. Gur, I. Ravina, A. J. Babchin, On the electrical double layer theory. II. the Poisson-Boltzmann equation including hydration forces, J. Colloid Interf. Sci. 64 (2) (1978) 333–341.
[25] J. R. Macdonald, Theory of the differential capacitance of the double layer in unadsorbed electrolytes, J. Chem. Phys. 22 (11) (1954) 1857–1866.
[26] H. Wang, J. Varghese, L. Pilon, Simulation of electric double layer capacitors with mesoporous electrodes: Effects of morphology and electrolyte permittivity, Electrochimica Acta 56 (17) (2011) 6189–6197.
[27] E. Glueckauf, Bulk dielectric constant of aqueous electrolyte solutions, Trans. Faraday Soc. 60 (1964) 1637–1645.
[28] D. Ben-Yaakov, D. Andelman, R. Podgornik, Dielectric decrement as a source of ion-specific effects, J. Chem. Phys. 134 (7) (2011) 074705.
[29] A. Levy, D. Andelman, H. Orland, Dielectric constant of ionic solutions: A field-theory approach, Phys. Rev. Lett. 108 (2012) 227801.
[30] A. Levy, D. Andelman, H. Orland, Dipolar Poisson-Boltzmann approach to ionic solutions: A mean field and loop expansion analysis, J. Chem. Phys. 139 (16) (2013) 164909.
[31] B. Li, J. Wen, S. Zhou, Mean-field theory and computation of electrostatics with ionic concentration dependent dielectrics, Commun. Math. Sci. 14 (1) (2016) 249–271.
[32] J. Bikerman, Structure and capacity of electrical double layer, The London, Edinburgh, and Dublin Philosophical Magazine and Journal of Science 33 (220) (1942) 384–397.
[33] M. Hatlo, R. Van Roij, L. Lue, The electric double layer at high surface potentials: The influence of excess ion polarizability, EPL (Europhysics Letters) 97 (2) (2012) 28010.
[34] Y. Nakayama, D. Andelman, Differential capacitance of the electric double layer: The interplay between ion finite size and dielectric decrement, J. Chem. Phys. 142 (4) (2015) 044706.
[35] D. J. Bonthuis, S. Gekle, R. R. Netz, Dielectric profile of interfacial water and its effect on double-layer capacitance, Phys. Rev. Lett. 107 (2011) 166102.
[36] D. J. Bonthuis, S. Gekle, R. R. Netz, Profile of the static permittivity tensor of water at interfaces: Consequences for capacitance, hydration interaction and ion adsorption, Langmuir 28 (20) (2012) 7679–7694.
[37] D. J. Bonthuis, R. R. Netz, Beyond the continuum: How molecular solvent structure affects electrostatics and hydrodynamics at solid-electrolyte interfaces, J. Phys. Chem. B 117 (39) (2013) 11397–11413.
[38] F. Fahrenberger, Z. Xu, C. Holm, Simulation of electric double layers around charged colloids in aqueous solution of variable permittivity, J. Chem. Phys. 141 (6) (2014) 064902.
[39] R. R. Netz, H. Orland, Beyond Poisson-Boltzmann: Fluctuation effects and correlation functions, Eur. Phys. J. E 1 (2000) 203–214.
[40] R. R. Netz, H. Orland, Variational charge renormalization in charged systems, Eur. Phys. J. E 11 (2003) 301–311.
[41] Z. G. Wang, Fluctuation in electrolyte solutions: The self energy, Phys. Rev. E 81 (2010) 021501.
[42] R. Wang, Z.-G. Wang, Effects of image charges on double layer structure and forces, J. Chem. Phys. 139 (2013) 124702.
[43] Z. Xu, M. Ma, P. Liu, Self-energy-modified Poisson-Nernst-Planck equations: WKB approximation and finite-difference approaches, Phys. Rev. E 90 (1) (2014) 013307.
[44] Z. Xu, A. Maggs, Solving fluctuation-enhanced Poisson-Boltzmann equations, J. Comput. Phys. 275 (2014) 310–322.

https://doi.org/10.4208/cicp.260715.210316a Published online by Cambridge University Press

[45] B.-S. Lu, X. Xing, Correlation potential of a test ion near a strongly charged plate, Phys. Rev. E 89 (2014) 032305.
[46] M. Ma, Z. Xu, Self-consistent field model for strong electrostatic correlations and inhomogeneous dielectric media, J. Chem. Phys. 141 (24) (2014) 244903.
[47] R. Wang, Z.-G. Wang, On the theoretical description of weakly charged surfaces, J. Chem. Phys. 142 (10) (2015) 104705.
[48] D. Gillespie, M. Valiskó, D. Boda, Density functional theory of the electrical double layer: the RFD functional, J. Phys. Condens. Matter 17 (42) (2005) 6609–6626.
[49] J. Jiang, D. Cao, D. Henderson, J. Wu, Revisiting density functionals for the primitive model of electric double layers, J. Chem. Phys. 140 (4) (2014) 044714.
[50] H.-J. Butt, K. Graf, M. Kappl, Physics and Chemistry of Interfaces, Wiley/VCH, Berlin, 2003.
[51] M. Paunovic, M. Schlesinger, Fundamentals of Electrochemical Deposition, Vol. 45, John Wiley & Sons, Hoboken, 2006.
[52] D. Frydel, Mean-field electrostatics beyond the point-charge description, Adv. Chem. Phys. 160 (2016) 209–260.
[53] L. Lin, C. Yang, J. Lu, L. Ying, W. E, A fast parallel algorithm for selected inversion of structured sparse matrices with application to 2D electronic structure calculations, SIAM J. Sci. Comput. 33 (3) (2011) 1329–1351.
[54] L. Lin, C. Yang, J. C. Meza, J. Lu, L. Ying, W. E, Selinv—An algorithm for selected inversion of a sparse symmetric matrix, ACM Trans. Math. Softw. 37 (2011) 40:1–40:19.
[55] D. C. Grahame, Differential capacity of mercury in aqueous sodium fluoride solutions. I. effect of concentration at 25°, J. Am. Chem. Soc. 76 (19) (1954) 4819–4823.
[56] L. Onsager, N. N. T. Samaras, The surface tension of Debye-Hückel electrolytes, J. Chem. Phys. 2 (1934) 528–536.
[57] Y. Levin, A. P. Dos Santos, A. Diehl, Ions at the air-water interface: an end to a hundred-year-old mystery?, Phys. Rev. Lett. 103 (25) (2009) 257802.
[58] R. Wang, Z.-G. Wang, Continuous self-energy of ions at the dielectric interface, Phys. Rev. Lett. 112 (13) (2014) 136101.
[59] P. Jungwirth, D. J. Tobias, Specific ion effects at the air/water interface, Chem. Rev. 106 (4) (2006) 1259–1281.
[60] D. C. Grahame, The electrical double layer and the theory of electrocapillarity, Chem. Rev. 32 (1947) 441–501.

https://doi.org/10.4208/cicp.260715.210316a Published online by Cambridge University Press